A rapid arousal brake on hunger neurons and its release in narcolepsy

Author list: Seher Kosar[1], Eva Bracey[1], Yihui Du[1], Daria Peleg-Raibstein[1], Denis Burdakov[1*]

Affiliations:

1. ETH Zürich: Department of Health Sciences and Technology (D-HEST); Neuroscience Center Zürich (ZNZ); Institute of Food, Nutrition and Health; Institute for Neuroscience. Schwerzenbach, Switzerland

* correspondence: denis.burdakov@hest.ethz.ch

ABSTRACT

Human sleep-wake disorders are often accompanied by eating disorders; the reasons for this apparent interplay between hunger and arousal remain unclear. Pupil-linked arousal fluctuates second-by-second, closely correlating with dynamics of hypocretin/orexin (H/O) neurons, whose malfunctions are linked to multiple pathologies. It is currently thought that H/O neurons activate hunger-causing agouti-related peptide (AGRP) neurons, thus creating concurrent arousal and hunger. Here, we directly measure pupil-linked arousal dynamics and concurrent AGRP neuron activity and find that, instead, pupil dilations correlate with reductions in AGRP neuron activity. Direct H/O neuron stimulation reproduced this inhibitory effect, while H/O neuron ablation attenuated it. Furthermore, in a mouse model of human type 1 (i.e. O/H deficient) narcolepsy, which involves unexplained overeating, we detected abnormal AGRP neuron hyperactivation during specific brain states, including the symptomatic shut-downs of arousal (cataplexy). Finally, we show that intact H/O neurons are required for normal food value perception by AGRP neurons, and for eating and AGRP neuron suppression by unexpected non-food stimuli. By demonstrating a rapid inhibitory H/O→AGRP influence and multiple pathophysiological consequences of its loss, these findings reveal a rapid functional link between arousal and hunger that is impaired by a neural defect associated with human disorders.

INTRODUCTION

Eating and sleep-wake disorders are highly prevalent in modern humans[1-4], leading to extensive investigations into the interplay between arousal and hunger states[5-11]. Homeostatic hunger is caused by agouti-related peptide/neuropeptide Y co-expressing neurons (AGRP neurons) in the hypothalamic arcuate nucleus[12-17]. AGRP neurons are activated by energy depletion[12-17], and inhibited by multiple aspects of feeding: rapid, "feedforward"[13] inhibition by food cues[18-20], slower inhibition by gut nutrients[21, 22], and even slower inhibition upon restoration of energy balance[13, 21]. The arousal-promoting/sleep-suppressing hypocretin/orexin -producing neurons[23-27] (H/O neurons) directly innervate AGRP neurons[28], and the H/O neurotransmitters rapidly (secs-mins) activate AGRP neurons[29, 30], leading to models[31-33] implying that the hunger signals are rapidly generated by the arousal signals (Fig. 1a).

However, such models fail to explain phenomena where feeding and arousal appear to change in opposite directions. For example, the human disorder type 1 narcolepsy involves a loss of H/O neurons but increased eating[9, 10] (up to 4 times of normal[34]). In turn, during ageing, there are reports of both an overall decline in food intake ("the anorexia of ageing"[35]), and of difficulties of falling and staying asleep[36, 37], recently linked to ageing-associated hyperexcitation of H/O neurons[38]. Furthermore, in anorexia, there are reports of increased wakefulness and arousal[5, 11].

Therefore, here we re-examined the functional relationship between rapid fluctuations in arousal, H/O neurons and AGRP neurons, focusing on time-resolved fluctuations of arousal and consciousness states, H/O neuron hyperexcitation, and AGRP dynamics in a model of type 1 (i.e. H/O-deficient[39]) human narcolepsy. We present evidence for a rapidly-acting arousal brake on hunger signals, and propose a new model for hunger-arousal interplay.

RESULTS

Momentary pupil dilations correlate with reductions in AGRP neuron activity

We first tested how AGRP neuron activity is temporally related to pupil size, a widely-used indicator of momentary arousal that combines multiple sources of neurocognitive information into a one-dimensional metric (reviewed in [40]). Pupil-linked arousal fluctuates rapidly and closely matches the natural activity dynamics of H/O neurons [24]. Contrary to the mainstream model that predicts positive co-modulation of H/O-linked arousal and AGRP activity (Fig. 1a), we found pupil size to be negatively correlated with AGRP activity (Fig. 1b-d). As expected from activation of AGRP neurons by energy depletion[12, 13], the dilation-associated AGRP inhibitions were clearly seen in fasted mice (Fig. 1c-f), but less so in fed mice where AGRP neurons are expected to already be inhibited (Supplementary Fig 1, see "Methods: Experimental conditions table").

Since pupil dilations correspond to H/O neuron activations[24], we therefore next explored a new hypothesis: that H/O neurons exert a non-canonical inhibitory influence on AGRP neurons, which contributes to dilation-associated AGRP neuron inhibition. This hypothesis predicts that H/O neuron activation elicits AGRP neuron inhibition, and that H/O neuron loss elevates AGRP neuron activity.

H/O neurons are capable of rapid inhibition of AGRP neurons

To test the first prediction, we selectively optostimulated H/O neurons by expressing the excitatory optoactuator ChrimsonR under the control of orexin promoter[41] (Fig. 2a). We first analyzed responses of individual arcuate AGRP neurons *in vitro*, in acute hypothalamic slices. We found that, among AGRP neurons that responded to the optostimulation, the responses were mostly inhibitory (Supplementary Fig. 2b-c). We reasoned that this inhibition may came from arcuate-projecting inhibitory neurons activated by the H/O neuron optostimulation, since AGRP neurons do not directly respond to the only inhibitory transmitter made by H/O neurons, dynorphin[42-45]. Arcuate-projecting VGAT neurons that inhibit AGRP neurons have been described in the mediodorsal hypothalamus[46]. We therefore anatomically mapped the responses to H/O neuron optostimulation of ARC-projecting (GCaMP retro-labelled) VGAT-cre neurons around mediodorsal hypothalamic area (Supplementary Fig. 2d). This confirmed strong optostimulation-induced excitation in a subset of arcuate-projecting VGAT neurons (Supplementary Fig. 2e,f).

To resolve how the H/O neuron stimulation influences AGRP neurons *in vivo*, we then recorded AGRP-GCaMP population activity using fiber photometry in freely-moving mice (Fig. 2b,c). We found that AGRP neuron activity was inhibited upon H/O neuron optostimulation in a stimulation-frequency dependent manner (Fig. 2b,c). These results thus suggest that – in agreement with our hypothesis – H/O neuron activity can inhibit AGRP neurons *in vivo*.

AGRP neuron inhibition during spontaneous pupil dilations requires H/O neurons

To test the second prediction of our hypothesis, we compared pupil-associated AGRP neuron activity in mice with selectively ablated H/O neurons[47-49] vs control mice with intact H/O neurons (Fig. 2d). We observed a significantly weakened negative correlation

between pupil size and AGRP neuron activity in H/O neuron ablated mice (Fig. 2e,f). To visualize effects more directly, we peak-aligned individual pupil dilations in H/O ablated and control mice, and examined associated AGRP neuron dynamics (Fig. 2e,f). This revealed significantly reduced dilation-associated AGRP neuron inhibition in the H/O neuron ablated mice (Fig. 2g,h). Overall, the data in Fig. 2 thus identify H/O neurons as important mechanistic mediators of inhibitory coupling between pupil dilation and AGRP neuron activity.

AGRP neuron hyperactivity during cataplexy in a mouse model of type 1 narcolepsy

Type 1 narcolepsy is a human neurological disorder involving abnormal sleep-wake fragmentation; this disorder is caused by loss of H/O neurons [39, 50]. H/O neurons normally display brief (sec-min) increases in activity during both wakefulness[51-58] and sleep[51, 59-61]. Based on our data, we hypothesized that these H/O neuron activations may limit AGRP neuron activity, and thus, in brains without H/O neurons, AGRP neurons may be hyperactive during certain brain states.

When we analyzed spontaneous phasic activations of AGRP neurons, we indeed found their amplitudes to be higher in H/O neuron ablated than in control mice (Fig. 3a-e). To define brain states corresponding to these aberrant AGRP hyperactivations, we used electroencephalogram-electromyography (EEG-EMG). Of particular clinical interest in type 1 narcolepsy are symptoms known as cataplexy, defined by cessation of motor activity, postural collapse, and entry into a theta oscillation-rich, "REM sleep-like" state directly from wakefulness [39, 62]. It remains unclear whether cataplexy episodes relate to hunger signals, which are presumably increased in narcolepsy patients since they overeat[9, 10, 34]. Our orexin-DTR mouse model of H/O neuron loss exhibits both overeating[47, 48] and cataplexy-like episodes (Fig. 3g,h). When we used established EEG-EMG-video criteria to identify cataplexy episodes, we noticed that large spikes in AGRP neuron activity coincide with the episodes (Fig. 3g,i). At a higher temporal resolution, we observed that AGRP neuron activity sharply increased during episode onsets, and fell back shortly after their offset (Fig. 3h,i).

We also systematically examined AGRP neuron activity corresponding to normal brain states (wakefulness, REM sleep, NREM sleep) (Fig. 3 and Supplementary Fig. 3). We identified pronounced increases in AGRP neuron activity during REM sleep (Fig. 3j-l). These REM-associated AGRP neuron activations were present in both control and H/O neuron ablated mice, but – as expected from removal of an input from H/O neurons [51, 60, 61]- were increased in amplitude in the H/O neuron ablated mice (Fig3k,l).

Together, these data reveal that, as predicted by our hypothesis that H/O neurons exert an inhibitory influence on AGRP neurons, there is temporally-defined AGRP neuron hyperactivity in type 1 narcolepsy, that marks cataplexy episodes, as well as REM sleep.

Role for H/O neurons in suppression of hunger signals by external stimuli

So far, we showed that H/O neurons shape AGRP neuron activity during internal events such as spontaneous arousals, REM sleep, and cataplexy. Do H/O neurons also shape AGRP neuron responses to external occurrences that may be evolutionarily-important for the brain to process and respond to, such as unexpected noises or proximity of food? We

hypothesized that external stimuli that rapidly activate H/O neurons would inhibit AGRP neuron output in an H/O neuron-dependent manner. We designed two assays to investigate this hypothesis.

First, we noted that among H/O neuron-activating stimuli are unexpected loud noises [51, 63]. We designed a feeding assay during which such a noise was briefly played (Fig. 4a; we confirmed that this noise activated H/O neurons in Supplementary Fig. 4a). In agreement with our hypothesis, we found that the noise inhibited AGRP neurons, and reduced spontaneous food intake if played while the mouse was eating (Fig. 4b-d, control mice). These AGRP neuron and behavioral responses were significantly reduced in H/O neuron ablated mice (Fig. 4b-d).

Second, we noted that AGRP neurons are known to be rapidly inhibited by food proximity. This response - termed feedforward inhibition [13] - occurs before the food is touched or digested, based on food sensory cues [18-20]. Because H/O neurons are also activated by sensory cues related to food[64, 65] (Supplementary Fig. 4b), and contribute to AGRP neuron inhibition (Figs. 1-3), we tested whether they contribute to the feedforward AGRP neuron inhibition by food. Indeed, we found that the amplitude of AGRP neuron inhibition by presentation of a highly palatable food (milkshake) was greatly reduced in H/O neuron ablated mice (Fig. 4f). The feedforward inhibition of AGRP neurons by food is thought to reflect food value sensing, since its amplitude is proportional to caloric value of the food, with larger inhibition evoked by calorie-dense foods such as peanut butter than by chow [18]. We found that H/O neurons also displayed such responses, but in the opposite direction: they were strongly activated by presentation of peanut butter and less so of chow (Supplementary Fig. 4b). We hypothesized that these H/O responses may affect AGRP neurons and thus contribute to the AGRP neuron sensing of food value. Consistent with this, in mice lacking H/O neurons, the inhibitory responses of AGRP neurons to food presentation no longer discriminated between peanut butter and chow (Fig. 4g,h). In contrast, AGRP neuron modulation by internal feedback signals (“hunger hormone” ghrelin, nutrient depletion [18]) persisted in mice without H/O neurons (Supplementary Fig. 4c,d). This indicates that H/O neurons do not modulate all internal-state-dependent responses of AGRP neurons, but are more selectively involved in their ability to sense external cues.

DISCUSSION

Based on our findings, we propose the following model of rapid interactions between arousal and hunger. External stimuli rapidly activate H/O neurons[51-54, 66]. This increases multiple general aspects of arousal[23, 24, 40, 67], enabling the organism to optimally address incoming dangers or opportunities (reviewed in [31, 68-70]). During caloric deficiency states when AGRP neurons are most active[12, 13], these momentary arousals rapidly translate into inhibition of hunger-causing AGRP neurons. In the case of stimuli whose meaning is not yet clear, this H/O→AGRP inhibition may enable a rapid shift from feeding-focused state driven by AGRP neurons[13] to a general arousal state required to assess a new situation[40, 71]. In the case of food-related stimuli, the H/O→AGRP neuron inhibition would contribute to the rapid sensing of food value by AGRP neurons, which is thought to be important for optimal regulation of ingestion[13, 72]. If it holds, this model implies an inhibitory interplay between momentary arousal and hunger states, which – possibly together with the slow modulation of AGRP neurons by circadian rhythms [73] - may explain eating and body weight consequences of H/O neuron loss, including in humans with type 1 narcolepsy [9, 10, 34]. Our findings in the mouse model of type 1 narcolepsy also document previously-missed neural dynamics during key symptoms: the AGRP neuron hyperactivation during cataplexy. Together, these observations thus open new avenues for understanding the full scope of this chronic neurological disorder, as well as other human disorders associated with loss of H/O neurons[74].

METHODS

Animal procedures

All procedures followed Swiss Federal Food Safety and Veterinary Office Welfare Ordinance (TSchV 455.1, approved by the Zurich Cantonal Veterinary Office), or the UK Home Office regulations. Adult (older than 22 weeks) female and male C57BL6 mice were used, sex is noted in Supplementary Table 1. Animals were housed in a 12-hour reversed light-dark cycle at 22°C with 55% humidity, and had ad libitum access to standard chow (3430 Kliba Nafag, Kaiseraugst, Switzerland) and water unless stated otherwise (Supplementary Table 1). AGRP-IRES-cre mice and VGAT-IRES-cre mice were from Jackson Lab (Jax no. 012899 and 028862, respectively). To study mice without H/O neurons, we selectively ablated H/O neurons using the previously validated hOrx-DTR mouse model[47] . To study AGRP neuron activity in H/O neuron ablated mice, AGRP-IRES-cre and orexin-DTR mice were crossed (AGRP-IRES-Cre x hOrx-DTR mice). Experiments were perfromed during the active (dark) phase of the light cycle, except for studies of sleep which were done during the inactive (light) phase (Fig. 3j-l and associated supplementary data).

Stereotaxic surgeries and viral vectors

Mice were anesthetized with 5% isoflurane, then transferred to the stereotaxic setup (Kopf Instruments, Tujunga, USA) and maintained on 1.5–2% isoflurane. They were given analgesic 30 mins before anaesthesia, and for three days post surgery. Lidocaine was applied to the scalp before an incision was made to access the cranium. Craniotomies were performed using a stereotax-mounted drill (RWD Life Sciences). Viral vectors and implants were positioned at specific coordinates (given below, as mm from Bregma unless stated otherwise). A Nanoject III injector was used to inject the viral vectors at a speed of 1 nl s^{-1}.

For AGRP neuron recordings, AAV9.CAG.Flex.GCaMP6s.WPRE.SV40 (titer ≥ 1.9×10^{13} vg/mL, from Addgene, MA, USA, 100842-AAV9) was injected unilaterally into the arcuate nucleus of AgRP-IRES-cre, or AgRP-IRES-cre x hOrx-DTR mice, at the following coordinates: anteroposterior -1.75, mediolateral -0.28, dorsoventral -6.1, -6.0 to -5.9 (100nl per site). Optic fibers (400 µm, 0.39 NA, 1.25 mm metal ferrule, Doric) were implanted at dorsoventral -5.85.

For H/O neuron recordings, AAV1.hORX.GCaMP6s.hGH (2.5×10^{12} GC ml^{-1}, Vigene Biosciences), previously demonstrated to selectively target H/O neurons[47], was injected at coordinates: anteroposterior -1.35, mediolateral -/+0.9, dorsoventral -5.7, 5.4 and 5.1 (50nl per site). A GRIN lens (ProView™ Integrated Lens 0.6mm x 7.3mm, Inscopix) was then implanted at dorsoventral -5.1.

For H/O neuron optostimulation, injection of AAV9-hORX-ChrimsonR-mCherry (2×10^{12} GC ml^{-1}, UZH Viral Vector Facility) previously demonstrated to selectively target H/O neurons[41], or control injection (PBS), was performed bilaterally at: anteroposterior -1.45, mediolateral ±2.8, dorsoventral -4.7 and -4.8 (150nl per site). For *in vivo* optostimulation of H/O neurons, optic fibers (200-µm diameter, 0.39 NA, 1.25-mm ceramic ferrule; Thorlabs), angled at a 20-degree angle from vertical, were placed 100 um above injection sites. For *in vitro* optogenetic-assisted probing of H/O→AGRP neuron

connectivity, AAV1-Syn-FLEX-GCaMP7f (Addgene, titer 1 × 10^{13}, 104492) was also injected into the arcuate nucleus (coordinates as above) of AgRP-IRES-cre mice.

For *in vitro* optogenetic-assisted calcium imaging probing functional connectivity from H/O neuron to arcuate-projecting VGAT neurons, we injected AAV9-hORX-ChrimsonR-mCherry into the lateral hypothalamus (coordinates as above) and AAVretro-Syn-FLEX-GCaMP7f (Addgene, at titer ≥v7×10^{12} vg/mL, catalog# 104492) into the arcuate nucleus (coordinates as above) of Vgat-IRES-cre mice.

For pupillometry, a custom-made headplate (Protolabs) was cemented to the skull.

For the electroencephalogram (EEG) and electromyogram (EMG) surgeries, a 3-channel EEG/EMG headmount (Pinnacle Technology, model 8235: 6-Pin Headmount, USA) was cemented to the skull and connected via stainless steel or copper wire to four stainless steel screws (Fine Science Tools) serving as cortical surface electrodes. The four screws were positioned at: (1) anteroposterior +1, mediolateral +1; (2) anteroposterior +1, mediolateral -1; (3) anterioposterior -4.5 and lateral +2, (4) from lambda: anteroposterior -1, mediolateral 0 (see Fig. 3). Screw (1) functioned as the ground connection. A pair of stainless steel/copper wires was implanted into the posterior neck muscle to capture EMG signals.

All implanted probes and headmounts were secured to the skull with three-part dental cement (Superbond, Sun Medical). Mice were allowed to recover from surgery for at least two weeks before experiments.

In vivo recordings of neural activity

Standard, dual-excitation-wavelength fiber photometry recordings and analyses (described in detail in previous work [66, 75, 76]) were used to obtain AGRP-GCaMP6s signals. H/O-GCaMP6s signals (Supplementary Fig. 4a,b) were obtained by whole-field imaging using an INSCOPIX head-mounted microscope, as described in detail in [66]. Fluorescence outputs were converted to normalised photometry signal % ΔF/F as described in [76-78]. Following guidelines in [79], for between-subjects visualisations, the % ΔF/F data were then converted to z scores using the function $z = (Fn - \mu)/\sigma$. Here, Fn is the normalized photometry signal, and μ and σ are the mean and standard deviation (respectively) of Fn of the whole recording session (Fig.1c, 3a, 3g, Supplementary Fig. 1a), or of a local baseline period around an event or a stimulus presentation (Fig.1e, 2g, 3h-k, 4a-h; Supplementary Figs except Supplementary Fig.1a). The local baseline period was -10 to -5 sec in 1e, 2g, Supplementary 1c; 20s of awake state in 3h,j; 25 sec before transition onset in 3k,l and Supplementary 3; and the pre-stimulus baselines depicted in remaining supplementary figures.

Combined pupillometry and neural activity recordings

Pupil dynamics in head-fixed mice allowed to run freely on a rotating wheel were recorded and analysed as previously described[24], using an infrared camera (Blackfly, FLIR Systems, Imaging software Spinnaker SDK, frame rate 30 Hz). Pupil boundaries were tracked using DeepLabCut to identify eight edge points in each video frame. A circle-fitting algorithm in MATLAB calculated pupil radius, enabling precise pupillary measurement across experimental conditions. Photometry and pupil size data were aligned and downsampled to 10 Hz using the function resample, and z-scored across the whole trace. To visualise

AGRP-GCaMP6s signals corresponding to similar pupil dilations in different mouse groups, dilation peaks were detected using findpeaks in Matlab (MinPeakProm=1SD) and events in which running was less than (0.05cm/sec) were removed. To analyse temporal correlations between AGRP-GCaMP6s signals and pupil size, AGRP events were detected using findpeaks in Matlab (min peak prominence 5% DF/F), time windows of 10s made around the peak of the event were taken, and cross-correlated with corresponding pupil data using the Matlab function xcorr with 'coeff' normalisation.

***In vivo* optogenetics**

Optogenetic stimulation of H/O neurons was performed as described in detail in our previous work [24]. In Fig. 2, 30 sec trains of 5 ms laser pulses at each of the stated frequences were applied at 3 minute intervals. Laser stimulation is repeated 3 times per indicated frequency, in Fig. 2C every line shows the average of responses to these repetitions for each frequency per mouse.

Brain slice recordings and optogenetics

300 µm hypothalamic coronal slices were acutely dissected and studied similarly to our previous work [44, 80-84]. Briefly, the slices were placed in a recording chamber of an Olympus microscope, continuously perfused with ACSF at 21°C, gassed with 95% O2 and 5% CO2. To stimulate ChrimsonR expressed in H/O neurons and axons, HEKA Patchmaster software was used to deliver 20 Hz, 30 sec trains of 5 ms pulses of a red laser (635 nm, Laserglow Technologies, 10mW at the fiber tip) through a fiberoptic tip (200 um diameter) placed above mediobasal or mediodorsal hypothalamic areas (defined in Supplementary Fig. 2). Calcium signals were recorded using a a UMPlanF l10x objective, Olympus (0.3 NA,10.10mm working distance) and Retiga ELECTRO camera (Imaging). Excitation light for calcium imaging was provided by a 1 Hz 465 nm Sutter Lambda 4DG light source, controlled by HEKA Patchmaster software. Images were acquired using HEKA SmartLUX and HEKA Patchmaster software. Regions of interest (ROIs) were manually labeled using ImageJ, and data were analyzed using MATLAB. Single-cell GCaMP signal was converted to z scores using mean and standard deviation of its baseline (30 sec before laser stimulation). If the z-score exceeded 1.5 SD for at least 5 seconds, the response was categorized as excitatory. Conversely, if the z-score was below -1.5 SD for at least 5 seconds, the response was categorized as inhibitory.

EEG/EMG recordings

EEG/EMG data were recorded similarly to our previous work [85, 86], using the Pinnacle tethered system and software (Pinnacle Technology, Lawrence, KS, USA). Signals were filtered by the preamplifier (high pass above 0.5 Hz for EEG and 10 Hz for EMG). Vigilance/sleep states (NREM, REM, and wake) were then automatically classified using an OSD4 script in Spike2 (CED, https://ced.co.uk/downloads/scriptspkanal), with 5-second epochs. After automatic detection, manual checking was also performed to ensure that the following criteria for EEG/EMG brain states were met: wakefulness was defined as desynchronized low-amplitude EEG and tonic EMG activity with phasic bursts; NREM sleep as synchronized, high-amplitude, low-frequency (1-4 Hz) EEG and reduced EMG activity compared with wakefulness with no phasic bursts; REM sleep as EEG with prominent theta power (4-9 Hz) and a flat EMG. For identification of cataplexy, videos of behavioral state were also recorded from above and beside the transparent recording

cage using 2 cameras (Basler acA1300-200um, Chromos Industrial). Video and EEG data were combined to identify cataplexy, as outlined in [87] (in brief: the cataplexy episodes were defined as an entry from wakefulness into a REM-like state with behavioral paralysis lasting lasting a minimum of 10 sec).

Lickometer analysis

Palatable food consumption was measured using a custom-built HPF dispenser (cat. no. 161K011, NResearch) with a capacitor-based lick sensor (cat. no. AT42QT-1010, SparkFun Electronics); data recorded at 500 Hz using custom Python scripts and a digital I/O device (NI-DAQmx, National Instruments), as in our previous work [48, 75]. As palatable food, we used milkshake (energy milk strawberry flavor, 0.76 kcal ml^{-1}, Emmi AG) because there is abundant evidence that it is highly attractive for both mice and humans [88-90]. 6 µl of HPF was dispensed for every 10 detected licks. In Fig. 4c, lick data was z scored to the local baseline period 5 sec before the sound stimulus.

Sudden noise experiments

Hungry mice (24 h fasted) were placed in a cage containing the lickometer dispensing milkshake. Mice were previously habituated to both lickometer and milkshake. After mice licked continuously for 30 sec, a white noise was played through a loudspeaker placed next to lickometer (1 sec duration, 120 dB), while licking and AGRP neuron responses were recorded (4b-d). To quantify the AGRP reponse to the noise without the confound of licking and moving around the case, AGRP responses were additionally recorded in the head-fixed setup (the same as used for pupillometry) without food (Fig. 4d).

Food presentation experiments

Animals were habituated to peanut butter (Migros Classic Crunchy, 6.04 kcal g^{-1}) and milkshake (energy milk strawberry flavor, 0.76 kcal ml^{-1}, Emmi AG) in home cages overnight and to experimental cages for a minimum of two days before experiments started. On experimental days, animals were placed in the experimental cage for 15 min and then different foods (peanut butter, milkshake, or their standard chow [Maintenace Standard diet]) were placed into the case as previously described [18].

Histology

In order to validate the locations of AAV virus expression and the fiber optic, we prepared 50 µm brain sections as described in [75], and aquired images using a fluorescence microscope (Eclipse Ti2, Nikon).

Data analysis and statistics

Data processing and statistical evaluations were conducted using MATLAB (Mathworks, USA). All animals and data points were included in the analyses, except for those with no signal in fiber photometry at the beginning of experiments. The results of all statistical tests are summarised in figure legends, and are fully specified in Supplementary Table 2. T-tests were two-tailed, except where alternative hypotheses were directional in which case one-tailed tests were used (as specified in Supplementary Table 2). P values less than 0.05 were deemed statistically significant. Results and figures are displayed as data mean ± SEM, unless stated otherwise.

ACKNOWLEDGEMENTS
This work was funded by ETH Zürich. We thank Mathilde Guillaumin and Han-Tao Li for their guidance on EEG/EMG surgery; Mathilde Guillaumin, Julia Harris, Bianca Viberti, and Micaela Borsa for their guidance on EEG/EMG data analysis for sleep scoring and narcolepsy episode identification; and Nikola Grujic for setting up and advising on pupillometry. We also thank Beate Laube for her help with mouse genotyping. We are grateful to Antoine Adamantidis and Markus Schmid, as well as Alexander Tesmer and Nikola Grujic, for helpful discussions and suggestions.

FIGURES

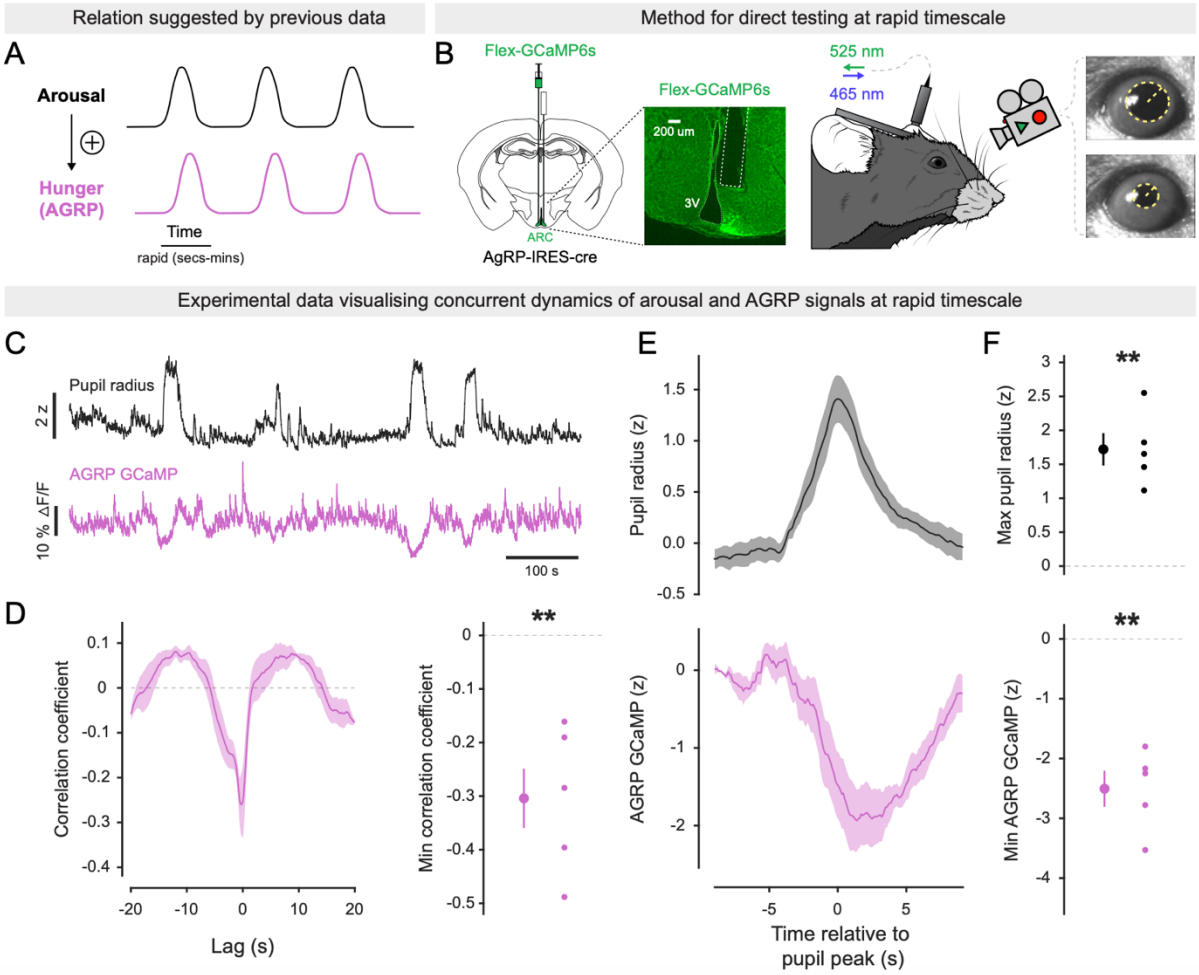

Fig. 1. Momentary pupil dilations correlate with reductions in AGRP neuron activity.

A. Previously-proposed relationship.
B. Method for direct experimental test of (A), including histology a coronal section showing example optical fiber and injection site.
C. Example recording of pupil radius and AGRP-GCaMP6s activity (representative trace of n = 5 mice).
D. Cross-correlation analysis of pupil radius and AGRP-GCaMP6s signal (mean of n = 5 mice). Right, quantification of correlation minima (n = 5 mice, ** p = 0.0079).
E. Pupil dilation events aligned with corresponding AGRP-GCaMP6s signals (152 events from n = 5 mice).
F. Quantification of data in (E), ** p = 0.0019 (pupil) and ** p = 0.0011 (AGRP). Throughout the figure: shaded areas or vertical bars show s.e.m.

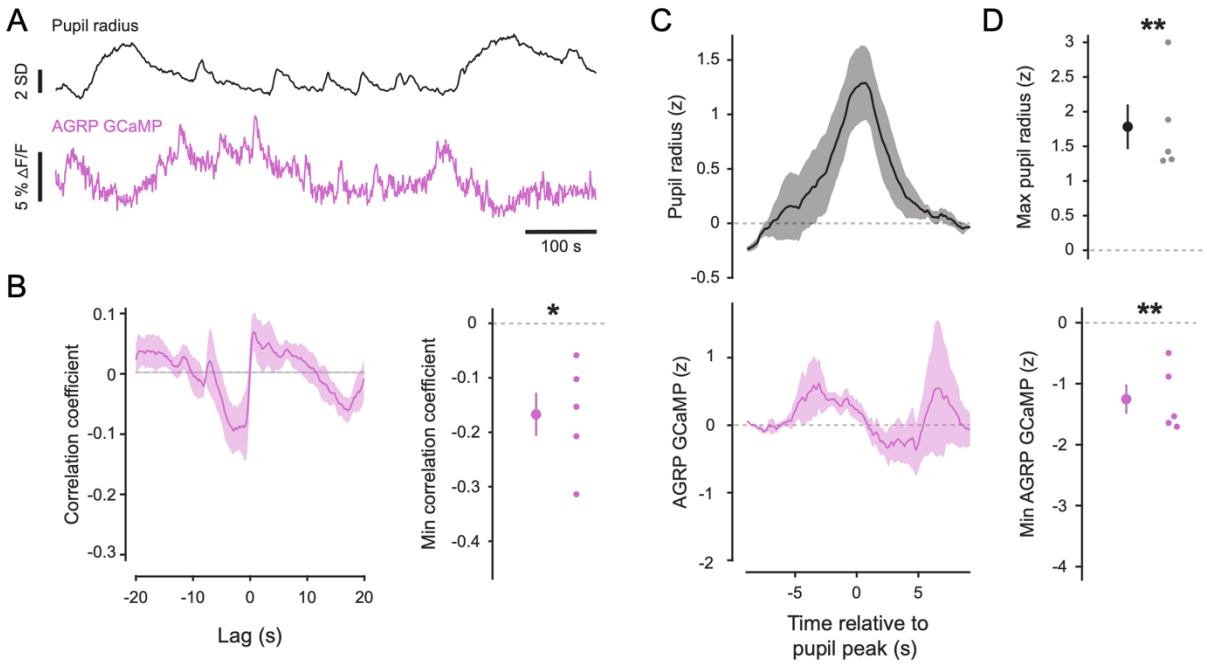

Supplemetnary Fig. 1. Pupil-AGRP neuron relations in ad lib fed mice.

A. Example recording of pupil and AGRP-GCaMP6s activity (representative trace of n = 5 ad libitum fed mice).
B. Cross correlation analysis of pupil radius and associated AGRP-GCaMP6s signals (n = 5 mice). Right, quantification of correlation minima (n = 5 mice,** P = 0.02).
C. Pupil dilation events aligned with corresponding AGRP-GCaMP6s signals (170 events from n = 5 mice).
D. Quantification of data in (C), ** P = 0.005 (pupil) and ** P = 0.006 (AGRP), n = 5 mice.

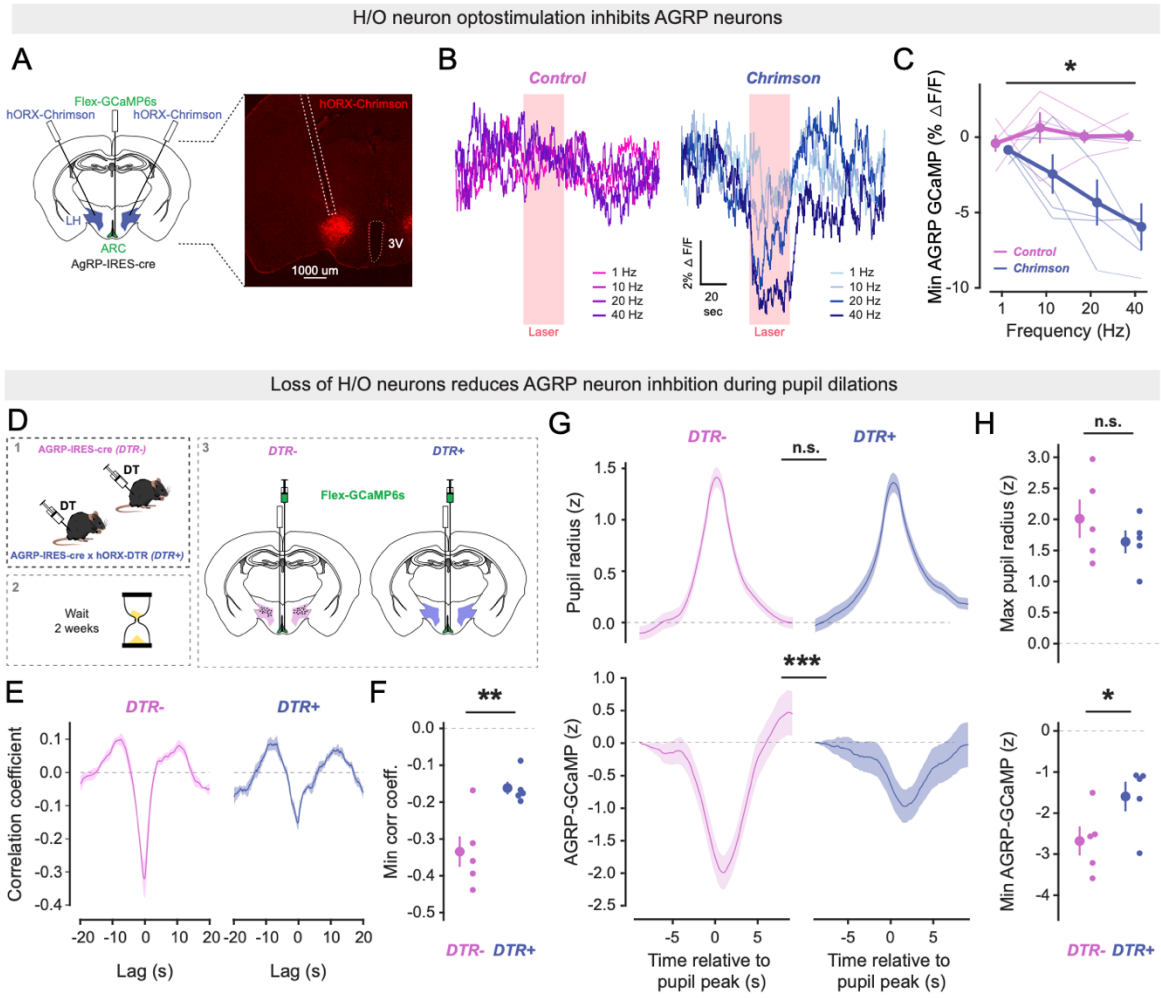

Fig. 2. Causal role for H/O neurons in rapid inhibition of AGRP neurons.

A. Left, targeting schematic for simultaneous H/O neuron optostimulation and AGRP neuron recording. Right, coronal section showing example optical fiber and injection sites.
B. AGRP-GCaMP6s responses to H/O neuron optostimulation (laser bar) at different frequencies (means of n = 5 mice in each dataset).
C. Quantification of (B) (frequency *P = 0.03; Chrimson vs. control *P = 0.02; n = 5 mice in each group).
D. Schematic for AGRP neuron recording in mice ablated of H/O neurons (DTR+) and control mice (DTR-).
E. Cross-correlation analysis of pupil radius and AGRP-GCaMP6s signals (n = 5 mice per group) in H/O neuron ablated (DTR+) and control (DTR-) mice.
F. Quantification of correlation minima from (E) (n = 5 mice in each group, ** P = 0.0086 .
G. Pupil dilation events (top) aligned with corresponding AGRP-GCaMP6s signals (bottom) in H/O neuron ablated (DTR+) and control (DTR-) mice (196 events from n = 5 DTR- mice, 172 events from n = 5 DTR+ mice). N.s. = P = 0.59; ***P<0.001 (comparison of means of -5 to +5 sec epochs).
H. Quantification of data in (G), top: n.s. = P= 0.166; bottom: *P=0.032 (n = 5 mice per group).

Throughout the figure: shaded areas or vertical bars show s.e.m.

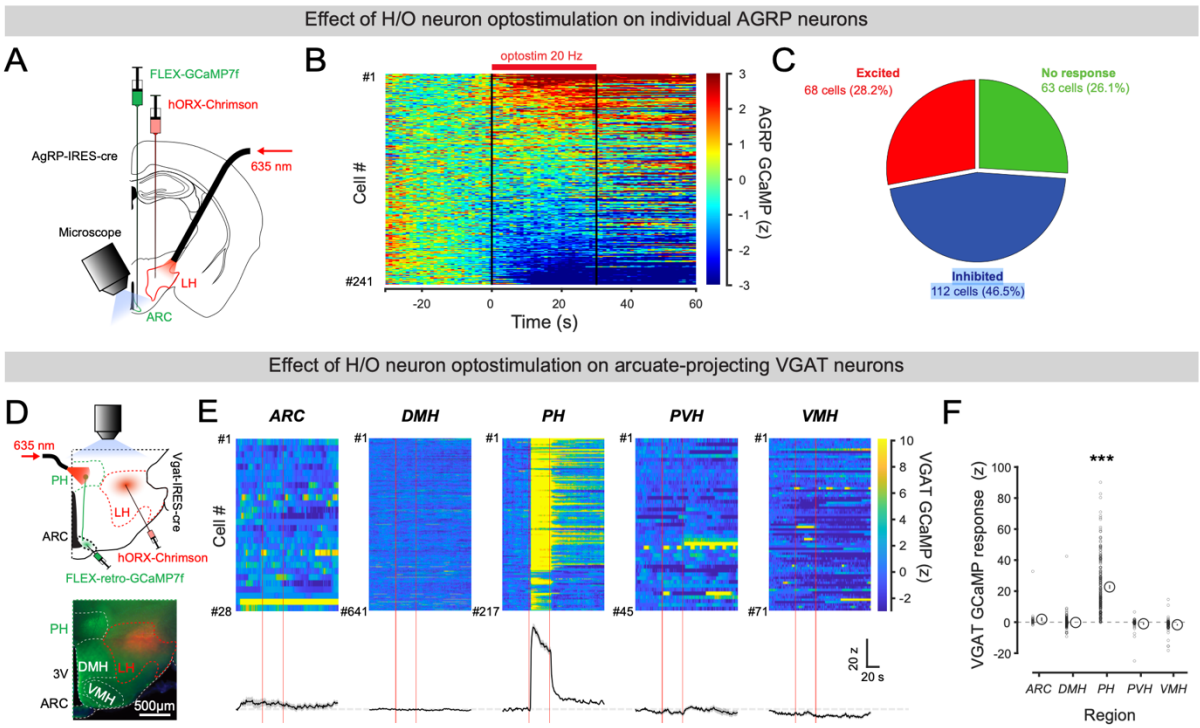

Supplementary Fig. 2. Single-cell analysis of responses to H/O neuron optostimulation of arcuate AGRP neurons and arctuate-projecting VGAT neurons.

A. Experimental design for single cell calcium imaging of AGRP-GCaMP7f and stimulation of H/O Chrimson neurons.
B. Heatmap shows single-cell AGRP responses to red laser stimulation of H/O neurons. Red bar indicates stimulation time (n=241 cells from 3 mice).
C. Characterisation of cells identified in (B). Cell activity was divided into three groups based on responses to H/O stimulation: Responses were either above (Excited cells), or below (inhibited cells) a threshold of 1.5 SD from the baseline for at least 5 seconds during laser stimulation. Cells with other responses were counted as "No response".
D. Top, Experimental design for single cell calcium imaging of AGRP-GCaMP7f and stimulation of H/O Chrimson axons in various nuclei. Bottom, Histology shows an example slice where the posterior hypothalamic nucleus (PH) responded to H/O neuron optical stimulation.
E. Top, Heatmaps displaying responses of GCaMP7f-expressing AGRP neurons to H/O Chrimson-expressing axon stimulation in different nuclei. Onset and offset of 635 nm laser stimulation is indicated by red lines.
   Coordinates for different nuclei were determined using The Mouse Brain in Stereotaxic Coordinates, Franklin & Paxinos, 1997, are listed in mm from bregma (AP, ML, DV) as follows:
   ARC, arcuate nucleus, -1.60 – 1.95, +/- 0.3, -5.9
   DMH - dorsomedial hypothalamic nucleus, -1.70-1.95, +/- 0.5, ~ -5.5
   PH - posterior hypothalamic nucleus, -1.85-1.95, -0.4, -4.75
   PVH - paraventricular hypothalamic nucleus -0.70-1, +/- 0.20, - 4.75
   VMH - ventromedial hypothalamic nucleus -1.60-1.95, +/- 0.5, -5.8
   Below, Average neuronal responses from heatmaps (n=3 mice).
F. Quanfication of population shown in (E, n = 214 cells, ***P < 0.0001).

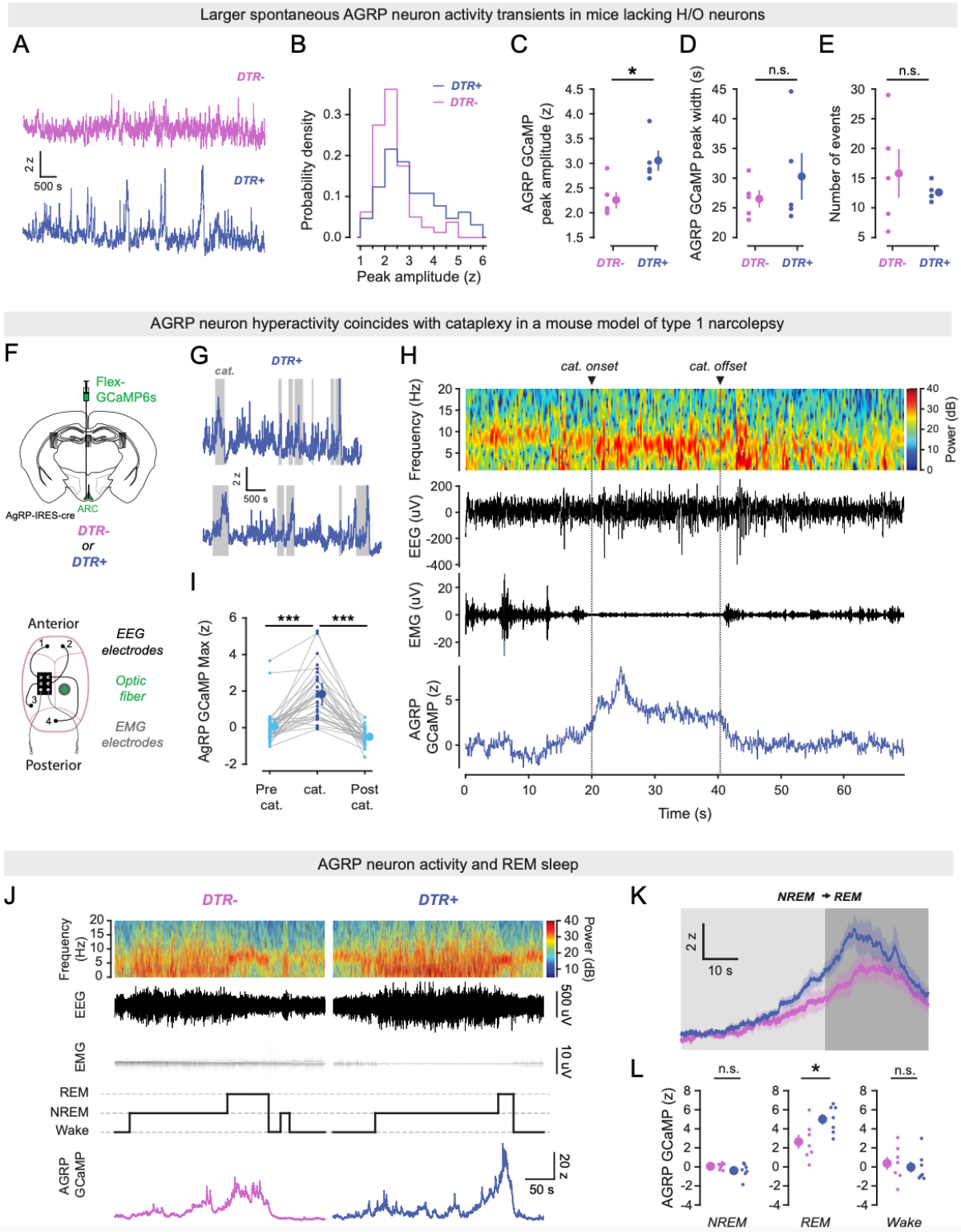

Fig. 3. Loss of H/O neurons causes AGRP hyperactivity during specific brain states.

A. Example recordings of spontaneous AGRP neuron activity in control (DTR-) and H/O neuron ablated (DTR+) mice (representative examples of n = 5 mice in each group).

B. Amplitude distributions of AGRP neuron activity spikes, showing a shift to larger amplitudes in DTR+ mice (***P= 0.000089, n = 5 mice in each group).

C-E. Qualification of the AGRP neuron spikes: peak amplitude (C), width (D), and number (E) (n=5 per each group, *P = 0.02, ns= P=0.39, 0.46, respectively).

F. Top, schematic of EEG/EMG recordigs and AGRP neuron recordings in H/O neuron ablated (DTR+) and control (DTR-) mice.

E. Examples of AGRP neuron activity during cataplexy episodes (cat., gray boxes) from a mouse lacking H/O neurons (DTR+); typical example of n = 5 mice.
F. A higher temporal resolution example of a cataplexy episode (cat.) showing temporal relations between (from top to bottom) EEG frequency power spectrum, raw EEG signal, raw EMG signal, and AGRP-GCaMP6s activity.
G. Quantification of AGRP neuron activity before/during/after cataplexy (5 seconds pre., 10 seconds post), n = 31 episodes from 5 H/O neuron ablated mice. ***P<0.0001.
H. Examples of a REM sleep event in H/O neuron ablated (DTR+) and control (DTR-) mouse, showing temporal relations between (from top to bottom) EEG frequency power spectrum, raw EEG signal, raw EMG signal, AGRP-GCaMP6s activity, and brain state hypnogram derived from EEG (REM=rapid eye movement sleep; NREM=non-rapid eye movement sleep).
I. Group data from experiment in J, showing AGRP-GCaMP6s signals aligned to transition into REM. Data show means and s.e.m of n = 7 DTR-, n= 7 DTR+ mice.
J. Quantification of AGRP-GCaMP6s activity associated with specific brain states (mean activity during 5-7 sec after transition) in H/O neuron ablated (DTR+) and control (DTR-) mice. *P=0.016, ns=P>0.05 (post-hoc tests following RM ANOVA).

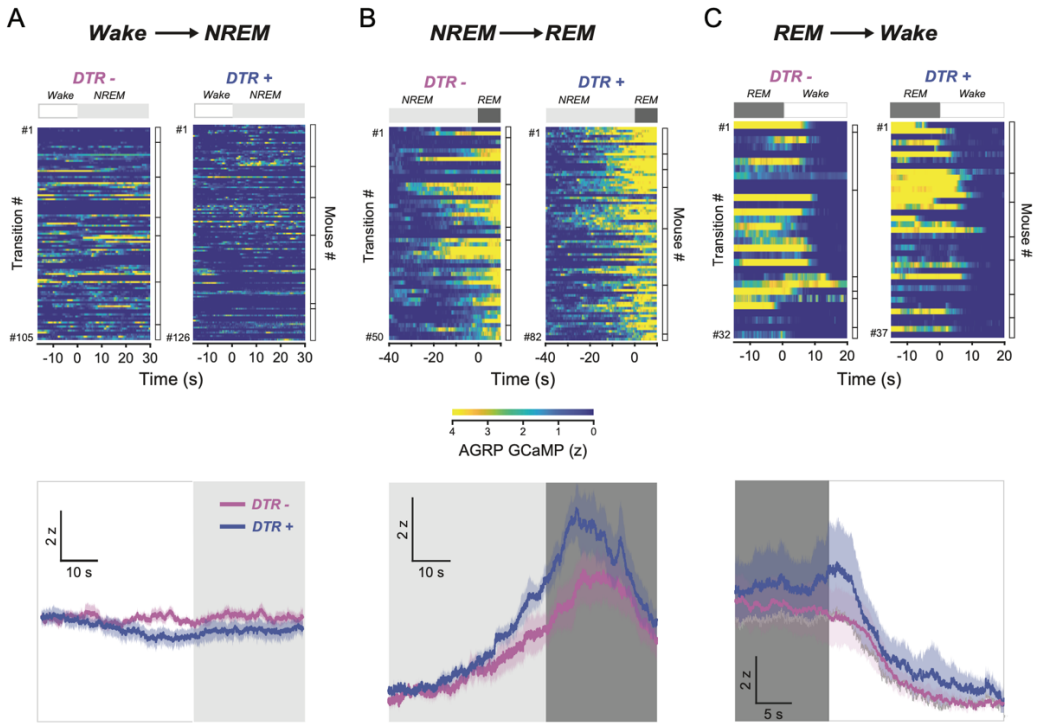

Supplementary Fig. 3. Additional data relating to Figure 3.

A. Top, AGRP activity during transitions from wake to NREM. Bottom, corresponding average traces of transition heatmaps.

B. As in A, for NREM to REM state (REM durations > 10 sec, NREM > 30 sec). Bottom, same trace as in main Fig. 3 (shown here again for consistency).

C. As in A, for REM to Wake transitions.

Data are means +/- SEM, n = 7 mice for each group across all panels.

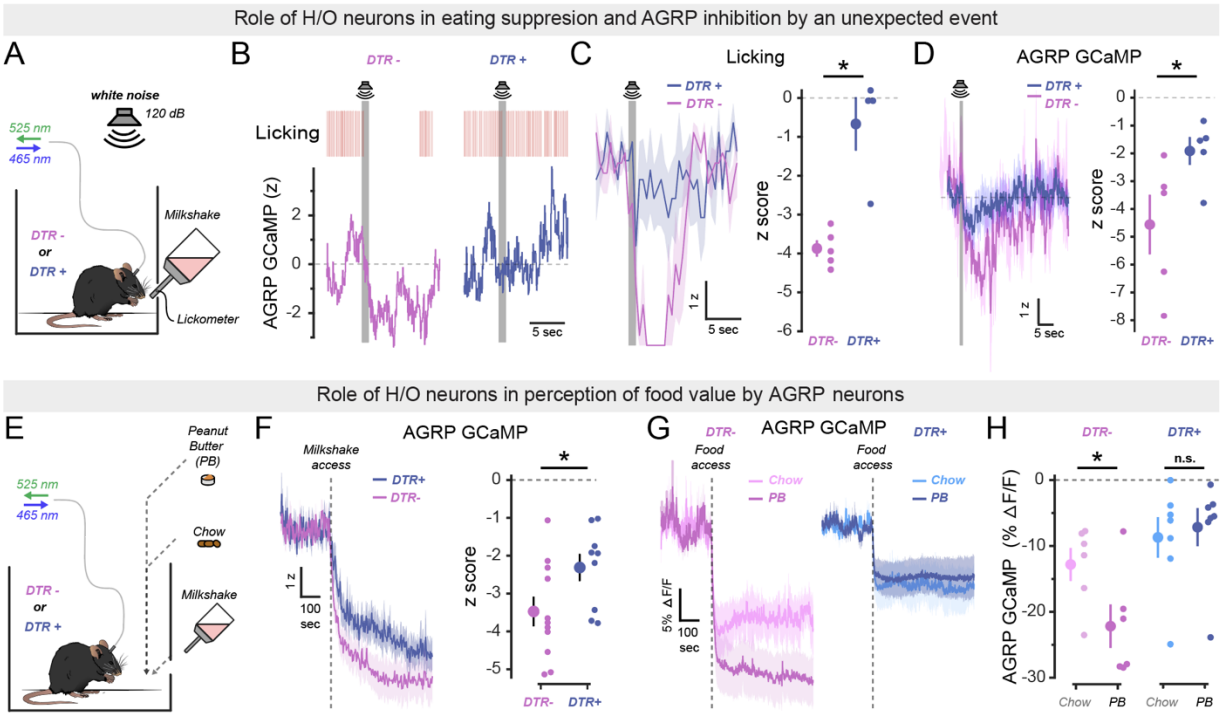

Fig. 4. Effect of H/O neuron ablation on rapid AGRP neuron responses to food and non-food stimuli.

A. Schematic of the "sudden noise" experiment used to obtain data shown in B-D.
B. Example effects on eating (top) and AGRP-GCaMP6s (bottom) of the noise (representative trace of DTR- n = 5 and DTR+ n = 4 mice).
C. Left: Group data for eating response show in B, mean of DTR- n = 5, DTR+ n = 4 mice. Right: Quantification, *P = 0.002).
D. Left: Group data for AGRP-GCaMP6s response, data are mean and s.e.m of n = 5 mice per group. Right: Quantification, *P = 0.01.
E. Schematic of the "food detection" experiment used to obtain data shown in f-h.
F. Left: AGRP neuron responses to presentation of a highly palatable food in H/O neuron ablated (DTR+, n = 9) and control (DTR-, n = 11) mice. Right: Quantification, *P=0.04.
G. AGRP neuron responses to presentation of peanut butter (PB, darker colours) vs chow (lighter colours) in H/O neuron ablated (DTR+) and control (DTR-) mice (data are mean and sem of n = 6 DTR-, n = 7 DTR+ mice).
H. Quantification of data in G. DTR-: chow vs palatable food *P=0.04; DTR+: chow vs palatable food P=0.30.

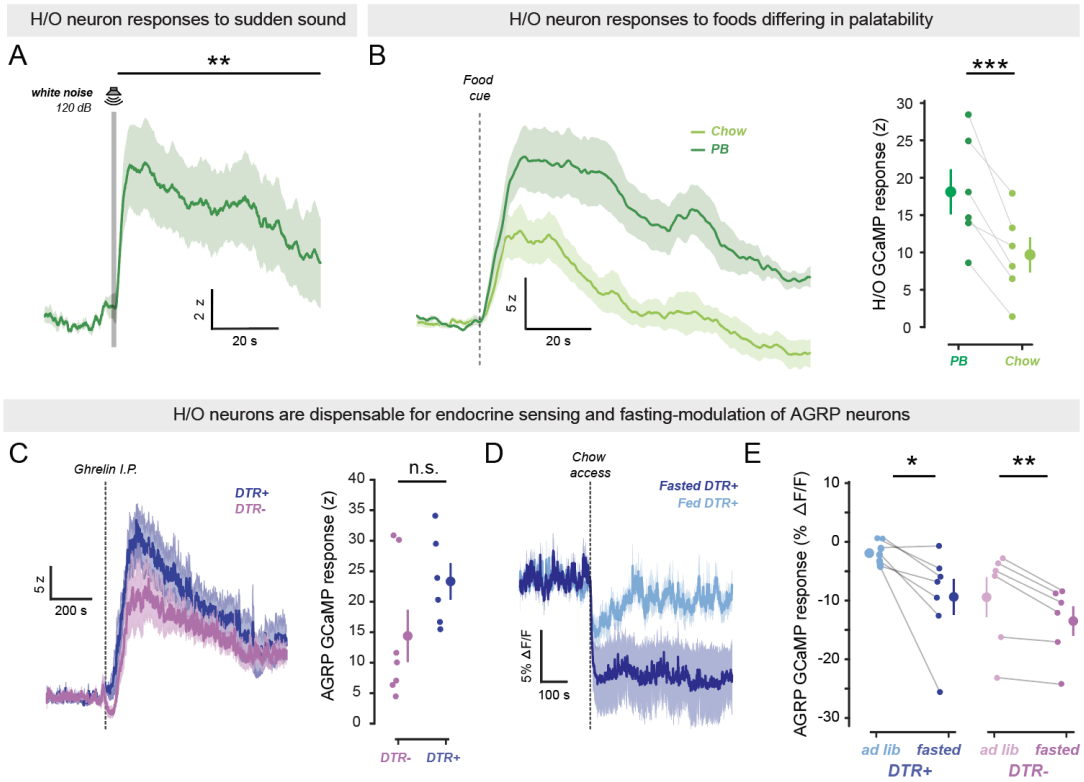

Supplementary Fig. 4. Additional data relating to main Fig. 4.
A. H/O neuron GCaMP responses to the sound stimulus used in Fig. 4 (n= 6 mice, **P = 0.003).
B. Left, H/O neuron responses to different food cues (PB = peanut butter). Right, Quantification of H/O neurons responses (n =6 mice, ***P = 0.0018).
C. Left, Comparison of AGRP neuron responses to ghrelin i.p. injection in DTR- vs. DTR+ mice. Right, quantification of responses to ghrelin (n = 4 DTR+, n = 6 DTR-; DTR+ vs. DTR-, ns = 0.125).
D. Left, Average AgRP neuron responses to chow in hungry (24h fasted) or ad lib fed H/O-ablated mice.
E. Left, Quantification of data in (D), *P = 0.03, **P = 0.01.

Supplementary Table 1. Summary of mice and nutritive states used in the study.
Mice were either ad lib fed or fasted as indicated in the table, for the following resons. H/O neuron optostimulation (Fig. 2) was done in fed mice, to avoid ceiling effects due to fasting-induced activation of H/O neurons. In sleep/wake studies (Fig. 3 and Supplementary Fig. 3) mice were fed to avoid effects of fasting on sleep states. In Fig. 4A-F mice were fasted to induce simular continous eating across mice. In Fig. 4G-K, mice were fasted to maximise AGRP neuron responses to food. Table 1 can be found at this link: https://polybox.ethz.ch/index.php/s/v8BVqzVTdfnD8If.

Supplementary Table 2. Statistical information.
Table 2 can be found at this link: https://polybox.ethz.ch/index.php/s/v8BVqzVTdfnD8If**.**

REFERENCES

1. Galmiche, M., Dechelotte, P., Lambert, G. & Tavolacci, M.P. Prevalence of eating disorders over the 2000-2018 period: a systematic literature review. *Am J Clin Nutr* **109**, 1402-1413 (2019).
2. Hauri, P.J. Sleep Disoders. in *Handbook of Psychology and Health, Volume 1* 211-260 (Routledge, 2021).
3. Ram, S., Seirawan, H., Kumar, S.K. & Clark, G.T. Prevalence and impact of sleep disorders and sleep habits in the United States. *Sleep Breath* **14**, 63-70 (2010).
4. Thorpy, M.J. Classification of sleep disorders. *Neurotherapeutics* **9**, 687-701 (2012).
5. Malcolm, A., Toh, W.L., Crocker, K. & Phillipou, A. The contribution of sleep to anorexia nervosa severity. *Eat Weight Disord* **27**, 1563-1568 (2022).
6. Allison, K.C., Spaeth, A. & Hopkins, C.M. Sleep and Eating Disorders. *Curr Psychiatry Rep* **18**, 92 (2016).
7. Olguin, P.*, et al.* Medical comorbidity of binge eating disorder. *Eat Weight Disord* **22**, 13-26 (2017).
8. da Luz, F.Q.*, et al.* A systematic review with meta-analyses of the relationship between recurrent binge eating and sleep parameters. *Int J Obes (Lond)* **47**, 145-164 (2023).
9. Baldini, V.*, et al.* Eating disorders in narcolepsy type 1: Evidence from a cross-sectional Italian study. *J Sleep Res* **33**, e14150 (2024).
10. Fortuyn, H.A.*, et al.* High prevalence of eating disorders in narcolepsy with cataplexy: a case-control study. *Sleep* **31**, 335-341 (2008).
11. Burger, P., Bos, R.W., Maas, J., Simeunovic-Ostojic, M. & Gemke, R. Sleep disturbances in anorexia nervosa. *Eur Eat Disord Rev* **33**, 318-342 (2025).
12. Hahn, T.M., Breininger, J.F., Baskin, D.G. & Schwartz, M.W. Coexpression of Agrp and NPY in fasting-activated hypothalamic neurons. *Nat Neurosci* **1**, 271-272 (1998).
13. Andermann, M.L. & Lowell, B.B. Toward a Wiring Diagram Understanding of Appetite Control. *Neuron* **95**, 757-778 (2017).
14. Aponte, Y., Atasoy, D. & Sternson, S.M. AGRP neurons are sufficient to orchestrate feeding behavior rapidly and without training. in *Nature Neuroscience* 351-355 (2011).
15. Gropp, E.*, et al.* Agouti-related peptide-expressing neurons are mandatory for feeding. *Nature Neuroscience* **8**, 1289-1291 (2005).
16. Krashes, M.J.*, et al.* Rapid, reversible activation of AgRP neurons drives feeding behavior in mice. *J Clin Invest* **121**, 1424-1428 (2011).
17. Luquet, S., Perez, F.A., Hnasko, T.S. & Palmiter, R.D. NPY/AgRP neurons are essential for feeding in adult mice but can be ablated in neonates. *Science* **310**, 683-685 (2005).
18. Chen, Y., Lin, Y.C., Kuo, T.W. & Knight, Z.A. Sensory detection of food rapidly modulates arcuate feeding circuits. *Cell* **160**, 829-841 (2015).
19. Betley, J.N.*, et al.* Neurons for hunger and thirst transmit a negative-valence teaching signal. in *Nature* 180-185 (Nature Research, 2015).
20. Mandelblat-Cerf, Y.*, et al.* Arcuate hypothalamic AgRP and putative POMC neurons show opposite changes in spiking across multiple timescales. *Elife* **4** (2015).

21. Beutler, L.R., *et al.* Dynamics of Gut-Brain Communication Underlying Hunger. in *Neuron* 461-475.e465 (Elsevier, 2017).
22. Su, Z., Alhadeff, A.L. & Betley, J.N. Nutritive, Post-ingestive Signals Are the Primary Regulators of AgRP Neuron Activity. *Cell Rep* **21**, 2724-2736 (2017).
23. Adamantidis, A.R., Zhang, F., Aravanis, A.M., Deisseroth, K. & de Lecea, L. Neural substrates of awakening probed with optogenetic control of hypocretin neurons. *Nature* **450**, 420-424 (2007).
24. Grujic, N., Tesmer, A., Bracey, E., Peleg-Raibstein, D. & Burdakov, D. Control and coding of pupil size by hypothalamic orexin neurons. *Nat Neurosci* **26**, 1160-1164 (2023).
25. Sakurai, T., *et al.* Orexins and orexin receptors: A family of hypothalamic neuropeptides and G protein-coupled receptors that regulate feeding behavior. *Cell* **92**, 573-585 (1998).
26. de Lecea, L., *et al.* The hypocretins: hypothalamus-specific peptides with neuroexcitatory activity. *Proc Natl Acad Sci U S A* **95**, 322-327 (1998).
27. De Luca, R., *et al.* Orexin neurons inhibit sleep to promote arousal. *Nat Commun* **13**, 4163 (2022).
28. Horvath, T.L., Diano, S. & van den Pol, A.N. Synaptic interaction between hypocretin (orexin) and neuropeptide Y cells in the rodent and primate hypothalamus: a novel circuit implicated in metabolic and endocrine regulations. *J Neurosci* **19**, 1072-1087 (1999).
29. van den Top, M., Lee, K., Whyment, A.D., Blanks, A.M. & Spanswick, D. Orexigen-sensitive NPY/AgRP pacemaker neurons in the hypothalamic arcuate nucleus. *Nature neuroscience* **7**, 493-494 (2004).
30. Muroya, S., *et al.* Orexins (hypocretins) directly interact with neuropeptide Y, POMC and glucose-responsive neurons to regulate Ca 2+ signaling in a reciprocal manner to leptin: orexigenic neuronal pathways in the mediobasal hypothalamus. *The European journal of neuroscience* **19**, 1524-1534 (2004).
31. Sakurai, T. The role of orexin in motivated behaviours. *Nat Rev Neurosci* **15**, 719-731 (2014).
32. Milbank, E. & Lopez, M. Orexins/Hypocretins: Key Regulators of Energy Homeostasis. *Front Endocrinol (Lausanne)* **10**, 830 (2019).
33. Tsujino, N. & Sakurai, T. Role of orexin in modulating arousal, feeding, and motivation. *Front Behav Neurosci* **7**, 28 (2013).
34. van Holst, R.J., *et al.* Aberrant Food Choices after Satiation in Human Orexin-Deficient Narcolepsy Type 1. *Sleep* **39**, 1951-1959 (2016).
35. Malafarina, V., Uriz-Otano, F., Gil-Guerrero, L. & Iniesta, R. The anorexia of ageing: physiopathology, prevalence, associated comorbidity and mortality. A systematic review. *Maturitas* **74**, 293-302 (2013).
36. Mander, B.A., Winer, J.R. & Walker, M.P. Sleep and Human Aging. *Neuron* **94**, 19-36 (2017).
37. Gulia, K.K. & Kumar, V.M. Sleep disorders in the elderly: a growing challenge. *Psychogeriatrics* **18**, 155-165 (2018).
38. Li, S.B., *et al.* Hyperexcitable arousal circuits drive sleep instability during aging. *Science* **375**, eabh3021 (2022).
39. Bassetti, C.L.A., *et al.* Narcolepsy - clinical spectrum, aetiopathophysiology, diagnosis and treatment. *Nat Rev Neurol* **15**, 519-539 (2019).

40. Grujic, N., Polania, R. & Burdakov, D. Neurobehavioral meaning of pupil size. *Neuron* (2024).
41. Duffet, L.*, et al.* A genetically encoded sensor for in vivo imaging of orexin neuropeptides. *Nat Methods* **19**, 231-241 (2022).
42. Li, Y. & van den Pol, A.N. Differential target-dependent actions of coexpressed inhibitory dynorphin and excitatory hypocretin/orexin neuropeptides. *The Journal of neuroscience : the official journal of the Society for Neuroscience* **26**, 13037-13047 (2006).
43. Chou, T.C.*, et al.* Orexin (hypocretin) neurons contain dynorphin. *J Neurosci* **21**, RC168 (2001).
44. Schöne, C., Apergis-Schoute, J., Sakurai, T., Adamantidis, A. & Burdakov, D. Coreleased orexin and glutamate evoke nonredundant spike outputs and computations in histamine neurons. *Cell Rep* **7**, 697-704 (2014).
45. Thomas, C.S.*, et al.* Optogenetic stimulation of lateral hypothalamic orexin/dynorphin inputs in the ventral tegmental area potentiates mesolimbic dopamine neurotransmission and promotes reward-seeking behaviours. *Neuropsychopharmacology* **47**, 728-740 (2022).
46. Garfield, A.S.*, et al.* Dynamic GABAergic afferent modulation of AgRP neurons. *Nat Neurosci* **19**, 1628-1635 (2016).
47. Gonzalez, J.A.*, et al.* Inhibitory Interplay between Orexin Neurons and Eating. *Current Biology* **26**, 2486-2491 (2016).
48. Viskaitis, P.*, et al.* Ingested non-essential amino acids recruit brain orexin cells to suppress eating in mice. *Curr Biol* **32**, 1812-1821 e1814 (2022).
49. Viskaitis, P.*, et al.* Orexin neurons track temporal features of blood glucose in behaving mice. *Nat Neurosci* **27**, 1299-1308 (2024).
50. Nishino, S., Ripley, B., Overeem, S., Lammers, G.J. & Mignot, E. Hypocretin (orexin) deficiency in human narcolepsy. *Lancet* **355**, 39-40 (2000).
51. Mileykovskiy, B.Y., Kiyashchenko, L.I. & Siegel, J.M. Behavioral correlates of activity in identified hypocretin/orexin neurons. *Neuron* **46**, 787-798 (2005).
52. Gonzalez, J.A., Iordanidou, P., Strom, M., Adamantidis, A. & Burdakov, D. Awake dynamics and brain-wide direct inputs of hypothalamic MCH and orexin networks. *Nat Commun* **7**, 11395 (2016).
53. Lee, M.G., Hassani, O.K. & Jones, B.E. Discharge of identified orexin/hypocretin neurons across the sleep-waking cycle. *J Neurosci* **25**, 6716-6720 (2005).
54. Giardino, W.J.*, et al.* Parallel circuits from the bed nuclei of stria terminalis to the lateral hypothalamus drive opposing emotional states. *Nat Neurosci* **21**, 1084-1095 (2018).
55. Bracey, E.F. & Burdakov, D. Fast sensory representations in the lateral hypothalamus and their roles in brain function. *Physiol Behav* **222**, 112952 (2020).
56. Burdakov, D. Subsecond Ensemble Dynamics of Orexin Neurons Link Sensation and Action. *Front Neurol Neurosci* **45**, 52-60 (2021).
57. Donegan, D.*, et al.* Hypothalamic Control of Forelimb Motor Adaptation. *J Neurosci* **42**, 6243-6257 (2022).
58. Donegan, D., Peleg-Raibstein, D., Lambercy, O. & Burdakov, D. Anticipatory countering of motor challenges by premovement activation of orexin neurons. *PNAS Nexus* **1** (2022).

59. Ito, H., *et al.* Deficiency of orexin signaling during sleep is involved in abnormal REM sleep architecture in narcolepsy. *Proc Natl Acad Sci U S A* **120**, e2301951120 (2023).
60. Broglia, G., *et al.* Hypothalamic control of noradrenergic neurons stabilizes sleep. *bioRxiv* (2024).
61. Feng, H., *et al.* Orexin signaling modulates synchronized excitation in the sublaterodorsal tegmental nucleus to stabilize REM sleep. *Nat Commun* **11**, 3661 (2020).
62. Hara, J., *et al.* Genetic ablation of orexin neurons in mice results in narcolepsy, hypophagia, and obesity. *Neuron* **30**, 345-354 (2001).
63. Takahashi, K., Lin, J.S. & Sakai, K. Neuronal activity of orexin and non-orexin waking-active neurons during wake-sleep states in the mouse. *Neuroscience* **153**, 860-870 (2008).
64. Petrovich, G.D., Hobin, M.P. & Reppucci, C.J. Selective Fos induction in hypothalamic orexin/hypocretin, but not melanin-concentrating hormone neurons, by a learned food-cue that stimulates feeding in sated rats. *Neuroscience* **224**, 70-80 (2012).
65. Hassani, O.K., Krause, M.R., Mainville, L., Cordova, C.A. & Jones, B.E. Orexin Neurons Respond Differentially to Auditory Cues Associated with Appetitive versus Aversive Outcomes. in *The Journal of Neuroscience* 1747 (Society for Neuroscience, 2016).
66. Karnani, M.M., *et al.* Role of spontaneous and sensory orexin network dynamics in rapid locomotion initiation. *Prog Neurobiol* **187**, 101771 (2020).
67. Yamashita, A., *et al.* Aversive emotion rapidly activates orexin neurons and increases heart rate in freely moving mice. *Mol Brain* **14**, 104 (2021).
68. Li, J., Hu, Z. & de Lecea, L. The hypocretins/orexins: integrators of multiple physiological functions. *Br J Pharmacol* **171**, 332-350 (2014).
69. Mahler, S.V., Moorman, D.E., Smith, R.J., James, M.H. & Aston-Jones, G. Motivational activation: a unifying hypothesis of orexin/hypocretin function. *Nat Neurosci* **17**, 1298-1303 (2014).
70. Burdakov, D. Reactive and predictive homeostasis: Roles of orexin/hypocretin neurons. *Neuropharmacology* **154**, 61-67 (2019).
71. de Araujo Salgado, I., *et al.* Toggling between food-seeking and self-preservation behaviors via hypothalamic response networks. *Neuron* (2023).
72. Chen, Y. & Knight, Z.A. Making sense of the sensory regulation of hunger neurons. *Bioessays* **38**, 316-324 (2016).
73. Sayar-Atasoy, N., *et al.* AgRP neurons encode circadian feeding time. *Nat Neurosci* **27**, 102-115 (2024).
74. Wang, C., *et al.* The Orexin/Receptor System: Molecular Mechanism and Therapeutic Potential for Neurological Diseases. *Front Mol Neurosci* **11**, 220 (2018).
75. Tesmer, A.L., *et al.* Orexin neurons mediate temptation-resistant voluntary exercise. *Nat Neurosci* **27**, 1774-1782 (2024).
76. Lerner, T.N., *et al.* Intact-Brain Analyses Reveal Distinct Information Carried by SNc Dopamine Subcircuits. *Cell* **162**, 635-647 (2015).
77. Kim, C.K., *et al.* Simultaneous fast measurement of circuit dynamics at multiple sites across the mammalian brain. *Nat Methods* **13**, 325-328 (2016).
78. Concetti, C., Bracey, E.F., Peleg-Raibstein, D. & Burdakov, D. Control of fear extinction by hypothalamic melanin-concentrating hormone-expressing neurons. *Proc Natl Acad Sci U S A* **117**, 22514-22521 (2020).

79. Sherathiya, V.N., Schaid, M.D., Seiler, J.L., Lopez, G.C. & Lerner, T.N. GuPPy, a Python toolbox for the analysis of fiber photometry data. *Sci Rep* **11**, 24212 (2021).
80. Schöne, C.*, et al.* Optogenetic probing of fast glutamatergic transmission from hypocretin/orexin to histamine neurons in situ. *J Neurosci* **32**, 12437-12443 (2012).
81. Kosse, C. & Burdakov, D. Natural hypothalamic circuit dynamics underlying object memorization. *Nat Commun* **10**, 2505 (2019).
82. Kosse, C. & Burdakov, D. Fast and Slow Oscillations Recruit Molecularly-Distinct Subnetworks of Lateral Hypothalamic Neurons In Situ. *eNeuro* **5** (2018).
83. Kosse, C., Schone, C., Bracey, E. & Burdakov, D. Orexin-driven GAD65 network of the lateral hypothalamus sets physical activity in mice. *Proc Natl Acad Sci U S A* **114**, 4525-4530 (2017).
84. Karnani, M.M.*, et al.* Activation of central orexin/hypocretin neurons by dietary amino acids. *Neuron* **72**, 616-629 (2011).
85. Li, H.T., Donegan, D.C., Peleg-Raibstein, D. & Burdakov, D. Hypothalamic deep brain stimulation as a strategy to manage anxiety disorders. *Proc Natl Acad Sci U S A* **119**, e2113518119 (2022).
86. Li, H.T., Viskaitis, P., Bracey, E., Peleg-Raibstein, D. & Burdakov, D. Transient targeting of hypothalamic orexin neurons alleviates seizures in a mouse model of epilepsy. *Nat Commun* **15**, 1249 (2024).
87. Willie, J.T.*, et al.* Distinct narcolepsy syndromes in Orexin receptor-2 and Orexin null mice: molecular genetic dissection of Non-REM and REM sleep regulatory processes. *Neuron* **38**, 715-730 (2003).
88. Bussey, T.J.*, et al.* New translational assays for preclinical modelling of cognition in schizophrenia: the touchscreen testing method for mice and rats. *Neuropharmacology* **62**, 1191-1203 (2012).
89. Kim, E.W.*, et al.* Optimizing reproducibility of operant testing through reinforcer standardization: identification of key nutritional constituents determining reward strength in touchscreens. *Mol Brain* **10**, 31 (2017).
90. Edwin Thanarajah, S.*, et al.* Habitual daily intake of a sweet and fatty snack modulates reward processing in humans. *Cell Metab* **35**, 571-584 e576 (2023).